# Electron Transport through Rectifying Self-Assembled Monolayer Diodes on Silicon: Fermi-Level Pinning at the Molecule−Metal Interface

**S. Lenfant,[†] D. Guerin,[†] F. Tran Van,[‡] C. Chevrot,[‡] S. Palacin,[§] J. P. Bourgoin,[||] O. Bouloussa,[⊥] F. Rondelez,[⊥] and D. Vuillaume*,[†]**

*Institut d'Electronique, Micro-électronique et Nanotechnologie, CNRS "Molecular Nanostructures & Devices" Group, BP 60069, avenue Poincaré, F-59652 Cedex, Villeneuve d'Ascq, France, Laboratoire de Physicochimie des Polymères et des Interfaces, Université de Cergy-Pontoise, 5 mail Gay Lussac, F-95031 Cergy-Pontoise, France, Chimie des Surfaces et Interfaces and Laboratoire d'Electronique Moléculaire, CEA Saclay, F-91191 Gif sur Yvette Cedex, France, and Laboratoire Physico-chimie Curie, CNRS, Institut Curie, 11 rue Pierre et Marie Curie, F-75231 Cedex 05, Paris, France*

*Received: June 28, 2005; In Final Form: May 16, 2006*

We report the synthesis and characterization of molecular rectifying diodes on silicon using sequential grafting of self-assembled monolayers of alkyl chains bearing a $\pi$ group at their outer end (Si/$\sigma$−$\pi$/metal junctions). We investigate the structure−performance relationships of these molecular devices, and we examine the extent to which the nature of the $\pi$ end group (change in the energy position of their molecular orbitals) drives the properties of these molecular diodes. Self-assembled monolayers of alkyl chains (different chain lengths from 6 to 15 methylene groups) functionalized by phenyl, anthracene, pyrene, ethylene dioxythiophene, ethylene dioxyphenyl, thiophene, terthiophene, and quaterthiophene were synthesized and characterized by contact angle measurements, ellipsometry, Fourier transform infrared spectroscopy, and atomic force microscopy. We demonstrate that reasonably well-packed monolayers are obtained in all cases. Their electrical properties were assessed by dc current−voltage characteristics and high-frequency (1-MHz) capacitance measurements. For all of the $\pi$ groups investigated here, we observed rectification behavior. These results extend our preliminary work using phenyl and thiophene groups (Lenfant et al., *Nano Lett.* 2003, *3*, 741). The experimental current−voltage curves were analyzed with a simple analytical model, from which we extracted the energy position of the molecular orbital of the $\pi$ group in resonance with the Fermi energy of the electrodes. We report experimental studies of the band lineup in these silicon/alkyl $\pi$-conjugated molecule/metal junctions. We conclude that Fermi-level pinning at the $\pi$ group/metal interface is mainly responsible for the observed absence of a dependence of the rectification effect on the nature of the $\pi$ groups, even though the groups examined were selected to have significant variations in their electronic molecular orbitals.

## I. Introduction and Motivation

As microelectronic devices approach their technological and physical limits,[1,2] molecular electronics, i.e., molecule-based information technology at the molecular scale, becomes increasingly investigated and envisioned as a promising candidate for the nanoelectronics of the future. In this respect, the supramolecular assembly of organic molecules on solid substrates is a powerful "bottom-up" approach for the fabrication of devices for molecular-scale electronics. A useful method is based on the self-assembly of monolayers of organic molecules on solid substrates (SAMs).[3] Many reports in the literature concern devices based on SAMs of thiol-terminated molecules chemisorbed on gold surfaces.[3−5] It is also valuable to develop and investigate molecular-scale devices based on SAMs chemisorbed on semiconductors, especially silicon. Silicon is the most widely used semiconductor in microelectronics, and a broad family of organic molecules can be grafted on its surface, which opens the possibility of tailoring the surface (e.g., modifying the surface potential)[6−8] for new and improved hybrid molecular/silicon devices. Between the end of the silicon road map and the envisioned advent of fully molecular-scale electronics, there is certainly a role to be played by such hybrid electronic devices.[2,9] Since the first adsorption from solution of alkyltrichlorosilane molecules on a solid substrate (mainly oxidized silicon) introduced by Bigelow, Pickett, and Zisman[10] and later developed by Maoz and Sagiv,[11] further detailed studies[12−15] have led to a better understanding of the basic chemical and thermodynamic mechanisms of this self-assembly process. Since the first study of the electronic properties of alkylsilane monolayers by Mann and Kuhn[16] and Polymeropoulos and Sagiv,[17] SAMs on silicon have been demonstrated to be high-quality ultrathin tunnel barriers[18,19] and have been used as gate dielectrics in nanometer-scale transistors.[20−22] SAMs of redox molecules (metallophorphyrines, ferrocene) have also been used as molecular memories[23,24] in hybrid CMOS/molecular DRAM circuits.[25] Molecular resonant tunneling diodes on silicon have also been demonstrated.[26]

Recently,[27] we demonstrated a molecular rectifying junction (MRJ) by attaching a donor group (phenyl or thiophene) to the alkyl spacer chain by a sequential grafting on silicon. We obtained rectification ratios of up to 35. We showed that the

* Corresponding author. E-mail: dominique.vuillaume@iemn.univ-lille1.fr.
† CNRS-Institut d'Electronique, Micro-electronique et Nanotechnologie.
‡ Université de Cergy-Pontoise.
§ Chimie des Surfaces et Interfaces, CEA Saclay.
|| Laboratoire d'Electronique Moléculaire, CEA Saclay.
⊥ CNRS, Institut Curie.

rectification mechanism is a resonance through the $\pi$ molecular orbital (ascribed to the highest occupied molecular orbital, HOMO) in good agreement with calculations and internal photoemission spectroscopy. This approach allowed us to fabricate molecular rectifying diodes compatible with silicon nanotechnologies for future hybrid circuitry. In this article, we present a systematic study of the synthesis, the structural and electrical properties of these rectifying molecular diodes, and we extend this work to a large number of chemically different $\pi$ end groups. The main objectives were to investigate the structure–performance relationships of these molecular devices and to examine the extent to which the nature of the $\pi$ end group drives their electrical properties. In this respect, SAMs of alkyl chains (chain lengths from 6 to 15 methylene groups) functionalized with a large variety of $\pi$-electron-rich chemical groups (phenyl, anthracene, pyrene, ethylene dioxythiophene, ethylene dioxyphenyl, thiophene, terthiophene, and quaterthiophene) were synthesized and characterized by contact angle measurements, ellipsometry, X-ray photoelectron spectroscopy (XPS), Fourier transform infrared (FTIR) spectroscopy, and atomic force microscopy (AFM). Their electrical properties were tested by dc current–voltage characteristics and high-frequency (1-MHz) capacitance measurements.

We chose a large number of $\pi$ groups having different molecular-orbital energy levels in the gas phase. We started with simple benzyl alcohol and 3-thiophenemethanol. Then, we moved from monomers to oligomers (terthiophene and quaterthiophene) and to fused oligoacenes (anthracene and pyrene). Our motivation was to establish a relationship between the electrical properties (electronic structure) of the starting $\pi$ molecules first in a vacuum and then when chemisorbed on the silicon substrate and to determine the current–voltage rectification behavior of the Si/molecule/metal junctions. From an engineering point of view, knowledge of this relationship is needed to design MRJs with electrical behavior suitable for device and circuit applications. For instance, in classical semiconductor p–n junctions, the threshold voltage for rectification is adjusted by doping, whereas here, it is envisioned that this could be done using chemistry, by changing the nature of the $\pi$ group.

It is known that charge transfer and band lineup [i.e., the energy position of the molecular orbitals (MOs) with respect to the Fermi energy of the electrodes] are the key parameters controlling the electronic properties of molecular devices.[28–31] This question has been addressed theoretically[28–31] in ideal metal–molecule–metal junctions with simple molecules (phenyldithiol, alkyl, alkane, and phenyl ethynylene). It is also known that the energy positions of the MOs of the gas-phase molecules and of the molecules in interaction with a surface are quite different. The energy levels of the MOs are broadened through hybridization with the delocalized wave functions of the metal electrodes, the energy levels are also shifted under the effects of fractional charge transfer at the interface, and the HOMO–LUMO gap can be substantially changed. As a typical example, two-photon photoemission experiments on SAMs of pentafluorothiophenolate chemisorbed on a Cu surface showed that the LUMO is downshifted by 3.1 eV and the HOMO is upshifted by 2.6 eV, leading to a HOMO–LUMO gap reduction of 5.6 eV compared to that of gas-phase molecules.[32] At the metal/organic semiconductor contact (as in organic light-emitting diodes), the breakdown of the vacuum alignment rule (Schottky–Mott model) was a major discovery in explaining the electronic properties of these devices,[33,34] and a large number of organic molecules deposited in ultrahigh vacuum (UHV) on

metal surfaces have been analyzed.[33,34] It has also been established that monolayers of molecules bearing a dipole moment can modify the electron affinity of semiconductor surfaces and, consequently, the metal/semiconductor Schottky barrier height.[35–37] In contrast, reports on molecular-scale junctions are scarce, probably because of the smaller number of investigated molecules and metal surfaces (much of the works have focused on gold surfaces with linear alkanes and linear $\pi$-conjugated oligomers). Moreover, in molecular junctions, the molecules are generally chemisorbed from solution or from the gas phase instead of being deposited under UHV conditions.

In this work, we report on a strong metal-induced Fermi-level pinning that completely controls the electrical behavior of the molecular rectifying diodes. To our knowledge, this feature has not been reported for silicon/SAM/metal junctions. In line with research cited above, we report this study to help in the understanding of the current–voltage rectification behavior of these Si/molecule/metal junctions.

## II. Experimental Section

On naturally oxidized silicon wafers bearing hydroxyl groups, SAMs are usually prepared from the reaction of molecules bearing a halo- or alkoxysilane headgroup [$Si–X_3$ with $X =$ Cl, $O(CH_3)_3$, $O(C_2H_5)_3$, etc.].[3,4] In general, it is desirable to introduce particular functionalities on the surface. Unfortunately, many such functionalities are not compatible with the silane (especially trichlorosilane) headgroups. Therefore, we used a sequential strategy. First, we began with the deposition of SAMs with relatively unreactive (i.e., relative to the trichlorosilane headgroup) end groups. Second, we modified the end groups (sequential grafting), following Wasserman et al., who reported the chemical transformation of vinyl-terminated SAMs into SAMs with carboxylic acid, alcohol, and bromide end groups.[38] These groups are prone to further surface modifications by other molecules.

**II.1. Step 1: Alkyl Chain Self-Assembled Monolayer Synthesis.** In this work, we used *n*-alkenyltrichlorosilane [$SiCl_3–(CH_2)_n–CH=CH_2$] with $n = 6$, 9, 12, and 15. The shorter molecules ($n = 6$ and 9), 7-octadecenyltrichlorosilane (OETS) and 10-undecenyltrichlorosilane (UETS), respectively, are commercially available (purchased from ABCR and used as received). The longer molecules ($n = 12$ and 15), 13-tetradecenyltrichlorosilane (TETS) and 16-heptadecenyltrichlorosilane (HETS), respectively, were synthesized according to the protocol developed by Bonnier[39] using enamine synthesis or by cross-linking the Grignard reagent of $\omega$-undecenyl bromide with the appropriate dibromoalkane to obtain the bromovinylic chain with the desired length. Addition of the $SiCl_3$ group was achieved by Grignard reaction of the alkenyl bromide with $SiCl_4$ (Figure 1). We also prepared SAMs with a methyl-terminated molecule, *n*-octadecyltrichlorosilane [OTS, $CH_3(CH_2)_{17}SiCl_3$], as a standard reference.

These alkyl-chain molecules were chemisorbed on naturally oxidized silicon substrates (1–1.5-nm-thick $SiO_2$ as measured by ellipsometry, vide infra) from a dilute solution ($10^{-2}$–$10^{-3}$ M) in an organic solvent [70/30% (v/v) hexane or hexadecane and carbon tetrachloride) using the method introduced by Bigelow, Pickett, and Zisman[10] and later developed by Maoz and Sagiv.[11] The silicon substrates (purchased from Siltronix) were degenerate n-type (resistivity of $\sim 10^{-3}$ $\Omega$ cm) to avoid any voltage drop in the substrate during electrical measurements. Prior to deposition, the substrates were carefully cleaned by extensive wet cleanings and dry cleanings by combining
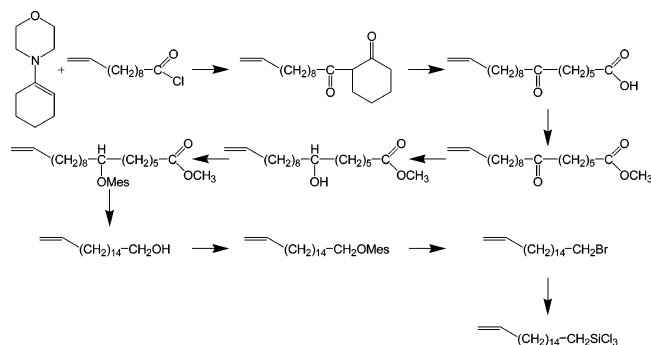
Electron Transport through Rectifying SAM Diodes on Si

*J. Phys. Chem. B, Vol. 110, No. 28, 2006* **13949**



**Figure 1.** Outline of the synthesis of the longer molecule, 16-heptadecenyltrichlorosilane (or HETS), according to Bonnier.[39]
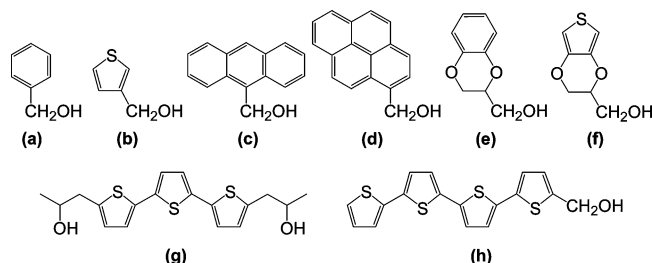


**Figure 2.** Chemical structures of compounds used to functionalize the SAMs: (a) benzyl alcohol, (b) 3-thiophenemethanol, (c) 9-anthracenemethanol, (d) 1-pyrenemethanol, (e) 3,4-ethylenedioxybenzene methanol (EDBM), (f) 3,4-ethylenedioxythiophene methanol (EDTM), (g) bis-(2-hydroxypropyl) terthiophene, and (h) hydroxymethyl quaterthiophene.

ultraviolet irradiation and ozone atmosphere. [The wet cleanings were performed mainly with piranha solution, 2/1 $H_2SO_4/H_2O_2$ (v/v). *Caution: Piranha solution is exothermic and strongly reacts with organics*.] The cleaned substrates were dipped into the freshly prepared solution, and the chemical reaction was allowed to proceed to completion. Typical reaction times were 90−120 min. We deposited HETS at 20 °C, TETS at 8 °C, UETS at 2 °C, and OETS at −20 °C; the corresponding critical temperatures ($T_c$) for optimum deposition (i.e., to form a densely packed and well-ordered monolayer) are approximately 26, 16, 6, and −10 °C, respectively. These critical temperatures were extrapolated from Brzoska et al.,[12,13] assuming that the critical temperatures for the vinyl-terminated alkyl chains were the same as for the methyl-terminated molecules used in their work. To control the solution temperature during the silanization reaction, the glass beaker was placed onto a cold plate (temperature controlled to within ±1 °C). To avoid any condensation of water when working at low temperature near the dew point of the atmosphere surrounding the reaction bath, we worked in a glovebox that was purged and maintained under a dry nitrogen flow (relative humidity of around 15%). The next step consisted of modifying the vinyl end groups by oxidation in $KMnO_4/NaIO_4/K_2CO_3$/deionized $H_2O$ [10/10/10/70% (v/v)] to obtain the COOH-terminated monolayers.[38] The oxidation time was 24 h at room temperature. For all of these chemical steps, we worked in a dry nitrogen-purged glovebox installed in a class 10000 clean room (temperature and relative humidity well controlled at 20 °C and 40%, respectively).[40]

**II.2. Step 2: Synthesis and Grafting of the π End Groups.** Finally, we grafted conjugated moieties onto the previously formed SAMs using esterification reactions between the −COOH end groups and several π-conjugated molecules bearing an alcohol group (R−OH). We started with simple benzyl alcohol and 3-thiophenemethanol (Figure 2a and b, respectively).[41] Then, we moved from monomers to oligomers, i.e., terthiophene and

quaterthiophene (Figure 2g and h), and to fused oligoacenes, i.e., anthracene and pyrene (Figure 2c and d).[42] Finally, we also used phenyl and thiophene derivatives substituted with ethylenedioxy (EDBM and EDTM, Figures 2e and f).

*Bis (5,5″-(2-hydroxy 2-methylethyl))-2,2′:5′,2″-terthiophene (3T; Figure 2g).* 2,2′:5′,2″-Terthiophene was first synthesized in diethyl ether using the well-known Grignard reaction from 2,5-dibromothiophene and 2-bromothiophene in the presence of Ni(II) catalyst (Nidpppcl$_2$).[43] mp (°C) 89. ^{1}H NMR (CDCl$_3$, ppm) 7.2 (H5,5″), 7.18 (H3,3″), 7.06 (H3′,4′), 7.0 (H4,4″). Five grams (20.1 mmol) of 2,2′:5′,2″- terthiophene were solubilized in dry diethyl ether, and 25.2 mL of butyllithium (2.5 M in hexane) was added. Stirring was maintained for 30 min at room temperature, and then 10 mL (143 mmol) of propyleneoxide was added dropwise. The resulting mixture was maintained under stirring for 3 h and then hydrolyzed with 30 mL of water. After filtration and extraction of the organic phase, the crude product was recrystallized in toluene, giving 2.2 g of brown crystals (yield 30%). mp (°C) 96.5. ^{1}H NMR (CDCl$_3$, ppm) 6.98 (H3′,H4′, H3,H3″), 6.75 (d, H4,H4″), 4.02 (m, 2H, CH$_2$-CHOHCH$_3$), 2.92 (m, 2H, **CH$_2$**CHOHCH$_3$), 1.72 (d, 2H, CH$_2$-CHO**H**CH$_3$), 1.28 (d, 6H, CH$_2$CHOHC**H$_3$**).

*2,3-Dihydrothieno[3,4-b]-1,4-dioxin-2-yl-methanol (or ethylene-dioxythiophene methanol, EDTM; Figure 2f)* was synthesized in six steps using a previously described procedure.[44−46]

*2-Hydroxymethyl-1,4-benzodioxan (or ethylenedioxybenzyl methanol, EDBM; Figure 2e).* Catechol (2.2 g, 20 mmol) was dissolved in 250 mL of boiling ethanol. Epibromhydrin (2.5 mL, 30 mmol) and potassium carbonate (0.55 g, 4 mmol) dissolved in 150 mL of water were then added. The mixture was heated at reflux for 1 h. Additional amounts of K$_2$CO$_3$ (0.3 g) and epibromhydrin (1 mL) were added. After being refluxed for 72 h, the solution was cooled and poured into 100 mL of acidified water (5% HCl). After the sample had been extracted with chloroform and dried over magnesium sulfate, the solvent was removed by evaporation under vacuum. Recrystallization in ether gave 2.1 g of white crystals (yield 63%). mp (°C) 88. ^{1}H NMR (CDCl$_3$, ppm) 6.87 (m, 4H), 4.26 (m, 2H), 4.1(m, 1H), 3.84(m, 2H), 1.91 (t, 1H).

The esterification was carried out for 120 h at room temperature (always in a class 10000 clean room and in the glovebox or in a dry nitrogen purged and sealed vessel) in the presence of DCCI (dicyclohexylcarbodiimide) to enhance the reaction yield (benzyl alcohol was used pure; the other compounds were dissolved in xylene at a concentration of 10$^{-2}$ M). The solution was renewed after 60 h to minimize its contamination and aging. Esterification for a shorter time led to poorer-quality SAMs as inferred from structural characterization (contact angle measurements, ellipsometry, FTIR spectroscopy, and AFM). Figure 3 shows schematic representations of these σ−π SAMs for each of the π groups.

**II.3. Wettability Measurements.** The contact angles of sessile drops of test liquids were measured using a remote computer-controlled goniometer system (DIGIDROP by GBX, France). A drop of deionized water (18 MΩ cm) or hexadecane (in the range of 1−10 μL) was deposited on the surface, and the projected image was acquired and stored on a remote computer. Contact angles were then extracted by contrast contour image analysis software. These static angles were determined within 5 s after application of the drop. These measurements were carried out in a clean room (class 1000) in which the relative humidity (40%) and the temperature (20 °C) were well controlled. The accuracy of these measurements was ±2°.
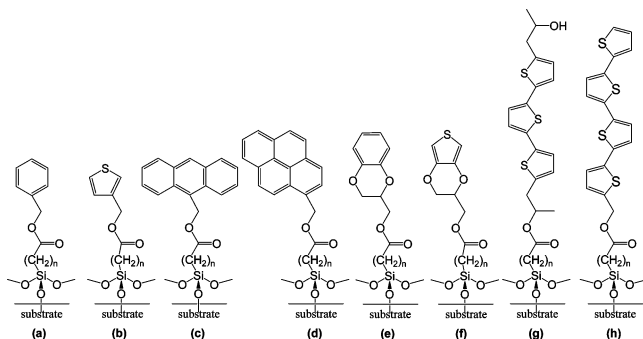
**Figure 3.** Schematic views of the final SAMs with the different aromatic molecules studied in this work: (a) benzyl alcohol, (b) 3-thiophenemethanol, (c) 9-anthracenemethanol, (d) 1-pyrenemethanol, (e) 3,4-ethylenedioxybenzene methanol (EDBM), (f) 3,4 -ethylenedi-oxythiophene methanol (EDTM), (g) bis-(2-hydroxypropyl) ter-thiophene, and (h) hydroxymethyl quaterthiophene.

## II.4. Thickness and Dielectric Constant Measurements.

The SAM thicknesses were measured by ellipsometry with a PLASMOS SD2300 instrument at 6328 Å. We used a value of $n = 1.50$ for the SAM refractive index at 6328 Å to calculate the thickness. Typical values in the literature are in the range of 1.45−1.50.[3] We also used a spectroscopic ellipsometer (UVISEL, Jobin Yvon) equipped with a DeltaPsi 2 data analysis software. The system acquired a spectrum ranging from 2 to 4.5 eV (corresponding to the range from 300 to 750 nm) at 0.05 eV (or 7.5 nm) intervals. Data were taken using an angle of incidence of 70°, with the compensator set at 45°. Data were fitted by regression analysis to a film-on-substrate model described by their thickness and their complex refractive indices. The optical parameters of the naturally oxidized substrate were independently determined by measuring a bare wafer rigorously cleaned by the same surface cleaning process (vide supra). The oxide layer thickness was found to be in the range 10−15 Å for all of the wafers used in this work. We compared the measured data with the simulated data to determine this thickness. The simulated data were obtained with a two-layer model: silicon substrate/silicon oxide. For Si and silicon oxide, we used the optical properties (complex refractive index for each wavelength) from the software library. After monolayer deposition, we used a three-layer model: silicon substrate/silicon oxide/organic monolayer. To determine the monolayer thickness, we fixed the oxide thickness at the previously measured value; for silicon and oxide, we again used the optical properties from the software library; and for the monolayer, we fixed the refractive index at 1.50. The accuracy of the SAM ellipsometry thickness measurements was estimated to be ±2 Å.

We also combined high-frequency (1-MHz) capacitance (vide infra) and ellipsometry to determine both the dielectric constant and the thickness of the SAMs. The SAM capacitance is given by $C_{SAM} = \epsilon_{SAM}\epsilon_0/d_{SAM}$, and the ellipsometry optical thickness is $K = nd_{SAM}$, where $\epsilon_0$ is the vacuum permittivity, $\epsilon_{SAM}$ is the relative SAM permittivity, $d_{SAM}$ is the SAM thickness, and $n$ is the SAM refractive index. Assuming that $\epsilon_{SAM} = n^2$, we calculated $\epsilon_{SAM}$, $n$, and $d_{SAM}$ using $d_{SAM} = (\epsilon_0 K^2/C_{SAM})^{1/3}$ and $n = (KC_{SAM}/\epsilon_0)^{1/3}$. These calculations neglect possible dipolar contributions to the dielectric function. This assumption was validated a posteriori by the fact that the measured thicknesses are in close agreement with the theoretical values (see section III.2).

## II.5. Fourier Transform Infrared Spectroscopy.

Fourier transform infrared (FTIR) spectroscopy measurements of the monolayers were done with a Perkin-Elmer Spectrum 2000 system, equipped with a liquid-nitrogen-cooled MCT detector.

We used internal reflection infrared spectroscopy (known as attenuated total reflection, ATR) and a silicon ATR crystal (10 mm × 5 mm × 1.5 mm, faces cut at 45°). All measurements were made after purging the sample chamber for 30 min with dry $N_2$. Spectra were recorded at 4 cm$^{-1}$ resolution, using strong apodization, and 200 scans were averaged to increase the signal-to-noise ratio. Background spectra were recorded on a freshly cleaned ATR crystal before each monolayer deposition.

## II.6. Atomic Force Microscopy.

We used atomic force microscopy (AFM) to image the surface morphology of the SAMs. We used a Nanoscope III (Digital Instruments) system in the tapping mode in air and at room temperature with a silicon tip. All images (512 × 512 pixels) were recorded at a scanning rate of 2−2.44 Hz. Surface regions from 50 × 50 nm to 5 × 5 $\mu$m were imaged.

## II.7. Electrical Measurements.

For the capacitance and conductivity measurements, we formed silicon/SAM/metal (SSM) heterostructures by evaporating metal (aluminum) through a shadow mask (electrode area = 10$^{-2}$ mm$^2$). To avoid contaminating the surface during metallization, an ultrahigh-vacuum (UHV) electron-beam evaporation system was used. It was verified that a 10$^{-8}$ Torr vacuum is innocuous for the SAMs. We have shown previously that such SAMs are thermally stable up to ∼350 °C in a vacuum;[47] nevertheless, during evaporation, the sample temperature was maintained below 50 °C. To avoid damage of the monolayer during the deposition of the first monolayers of the evaporated metal atoms, we used a low evaporation rate (1−5 Å/s) and a large distance between the sample and the crucible of metal (∼70 cm). The electrode thicknesses were in the range of 200−500 nm. More than 20 SSM devices were measured for each combination of alkyl chain lengths and $\pi$ end groups. The success rate for forming working junction was about 50−70% (ratio of non-short-circuited devices to complete measured ones). Aluminum (instead of gold) was chosen to avoid any rectification effect coming from the difference in the work functions of the two electrodes ($W_M \approx 4.2$ eV for Al and $W_{Si} \approx \chi_{Si} = 4.1$ eV for n$^+$-type Si, where $\chi_{Si}$ is the electron affinity), as it is well-known that a larger current is obtained when a positive bias is applied to the electrode with the smallest work function.[48] This effect was observed through metal/SAM/metal junctions with Au and Ti electrodes.[49]

The SSM structures were mounted onto a wafer chuck with silver paste to ensure good electrical contact with the silicon underlayer. The electrode was contacted with precision micro-manipulators. Electrical transport through the SAMs was determined by measuring the current density versus the applied dc voltage with an Agilent 4140B picoammeter. We used a low-speed steplike voltage ramp (step voltage = 10 mV, duration = 1.5 s) to avoid transient effects due to displacement current because the SSM junctions mainly act as capacitors. Capacitances were measured at 1 MHz (ac signal amplitude = 20 mV$_{eff}$) by an Agilent 4274A LCR meter. In both cases, voltages were applied to the metal counter electrode, the silicon substrate being grounded. The measurements were made at room temperature and in the ambient atmosphere. The SAM capacitance, $C_{SAM}$, was deduced from the measured capacitance, $C_{meas}$, taking into account the capacitance of oxides ($C_{ox}$) and the capacitance of the silicon substrate ($C_{sc}$): $1/C_{meas} = 1/C_{sc} + 1/C_{ox} + 1/C_{SAM}$. We modeled the degenerate semiconductor by its Debye capacitance, $C_{sc} = C_{Debye} = \epsilon_0\epsilon_{sc}/\lambda_{Debye}$, where $\epsilon_{sc}$ is the dielectric constant of the semiconductor (11.9 for silicon) and $\lambda_{Debye}$ is the extrinsic Debye length. The latter is given by $(\epsilon_0\epsilon_{sc}kT/q^2N_D)^{1/2}$, where $k$ is the Boltzmann constant, $q$ is the

Electron Transport through Rectifying SAM Diodes on Si

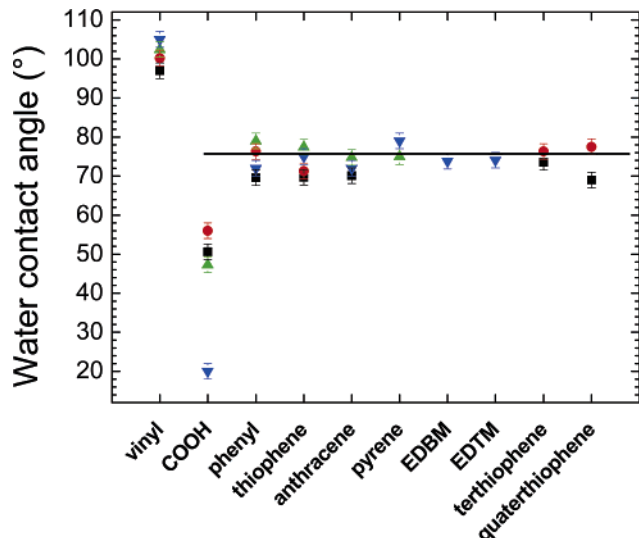*J. Phys. Chem. B, Vol. 110, No. 28, 2006* **13951**



**Figure 4.** Evolution of the water contact angles for the different chemical functionalizations of the SAMs for each molecule used for the silanization: HETS (▼), TETS (▲), UETS (●), OETS (■).

**TABLE 1: Contact Angles with Water ($\theta_{H_2O}$) and Hexadecane ($\theta_{HD}$) for Each Monolayer before and after Oxidation**

| | vinyl-terminated monolayer | | COOH-terminated monolayer | | |
|---|---|---|---|---|---|
| | $\theta_{H_2O}$ (deg) | $\theta_{HD}$ (deg) | $\theta_{H_2O}$ (deg) | $\theta_{HD}$ (deg) | $\eta_{ox}$ % |
| HETS | $105 \pm 2$ | $37 \pm 2$ | $20 \pm 2$ | $<10$ | $95 \pm 5$ |
| TETS | $102 \pm 2$ | $18 \pm 2$ | $47 \pm 2$ | $<10$ | $74 \pm 5$ |
| UETS | $100 \pm 2$ | $<10$ | $56 \pm 2$ | $<10$ | $63 \pm 5$ |
| OETS | $97 \pm 2$ | $<10$ | $50 \pm 2$ | $<10$ | $68 \pm 5$ |

*a* The yield of this reaction ($\eta_{ox}$) for each molecule was calculated by the Cassie Law (see text for details).

elementary electron charge, $T$ is the temperature, and $N_D$ is the doping concentration in the semiconductor (here $\sim 10^{19}$ cm$^{-3}$). We get $C_{Debye} \approx 8$ $\mu$F/cm$^2$. The oxide capacitance $C_{ox} = \epsilon_0\epsilon_{ox}/d_{ox}$ was calculated using the measured native oxide thickness (ellipsometry) and taking $\epsilon_{ox} = 3.9$.

## III. Results and Discussion

**III.1. Contact Angles.** Figure 4 summarizes the measured evolution of the water contact angles for the different chemical functionalizations of the SAMs. Table 1 lists the water and hexadecane contact angles measured on the alkyl-chain SAMs after and before the oxidation reaction. For the OTS monolayer used as a standard reference, the contact angles were $108° \pm 2°$ for water and $43° \pm 2°$ for hexadecane, as expected for a densely packed methyl-terminated SAM.[3,12,13] The vinyl-terminated SAMs were clearly hydrophobic, with $97° < \theta_{H_2O} < 105°$. The oxidation reaction makes them more hydrophilic, with $20° < \theta_{H_2O} < 56°$ depending on the length of the alkyl chains. After esterification with any of the $\pi$ groups, the water contact angles were always in the range of $70-80°$. Our contact angles for the vinyl-terminated monolayers value are in good agreement with earlier reports on similar systems.[3,50] For instance, Steel et al.[50] reported $\theta_{H_2O} = 108° \pm 3°$ and $\theta_{HD} = 39° \pm 3°$ for a vinyl-terminated alkylthiol SAM on gold (chain length of nine methylene groups). Both the water and hexadecane contact angle values compare well with those obtained in this work for the longest chain (HETS). Our hexadecane contact angles decrease with decreasing chain lengths from 15 to 6

methylene groups, becoming too low and unmeasurable ($<10°$) for the two shortest chains. This reflects a more disordered SAM for the short-chain molecules (see section 3.3 on FTIR results) and the fact that the underlying hydrophilic SiO$_2$ surface can contribute to the wetting properties for such a short chain.[51] After oxidation, the water contact angle should have been equal to $0°$ for a nearly ideal, 100% covered, COOH-terminated monolayer.[52] We measured higher values, indicating partial COOH surface coverage. Assuming that the monolayer surface is made of a mixture of vinyl and acid carboxylic moieties and using the Cassie law,[53] we estimated the oxidation reaction yield as

$$\cos \theta_{vin/carb} = r_{vin} \cos \theta_{vin} + r_{carb} \cos \theta_{carb} \tag{1}$$

where $\theta_{vin/carb}$ is the measured contact angle after oxidation; $r_{vin}$ is the relative surface coverage by vinyl groups; $r_{carb}$ is the relative surface coverage by COOH groups ($r_{vin} + r_{carb} = 1$); and $\theta_{vin}$ and $\theta_{carb}$ are the water contact angles for an ideal surface, fully covered by vinyl and COOH groups, respectively, for which we used $105°$ and $0°$, respectively. We obtained oxidation yields $\eta_{ox} = r_{carb}$ (assuming that $r_{vin} = 1$ for the monolayer before oxidation) of $68 \pm 5\%$, $63 \pm 5\%$, $74 \pm 5\%$, $95 \pm 5\%$ for the OETS, UETS, TETS, and HETS monolayers, respectively (Table 1). These yields are in agreement with data reported by Wasserman et al.,[38] who estimated the yield of this chemical surface modification to be in the range $70-90\%$. However, we notice that the shorter the chain length, the lower the water contact angle and the deduced oxidation yield. This can be explained by an increase in the disorder with decreasing chain length (see section 3.3 for FTIR confirmation), and thus we overestimated the oxidation yield because $r_{vin} < 1$ for the SAMs before oxidation. After esterification, the contact angles are in agreement with other reports on similar systems (monolayers functionalized with thiophene[54] and phenyl[50]). These values are also in agreement with those expected if the aromatic groups are densely packed and if they preferentially expose their edges to the probe liquid.[55]

**III.2. Ellipsometry.** Table 2 summarizes the thicknesses of the SAMs and provides a comparison with the expected value for a "near-perfect" densely packed SAM. The expected thickness corresponds to the length of the molecule, as given by PM3 geometry optimization with the CS-MOPAC software,[56] assuming that the main axis of the molecule is perpendicular to the surface substrate. We observed a relatively good agreement between the measured and expected values. The differences are always lower than 5 Å and can be ascribed to irreproducibility and sample-to-sample variations of the native oxide ($1-1.5$ nm). This indicates a reasonably good packing of these SAMs, especially after the grafting of the $\pi$ end groups.

In the case of the vinyl-terminated monolayers, we measured values of $12 \pm 2$, $17 \pm 2$, $18 \pm 2$, and $26 \pm 2$ Å for the OETS, UETS, TETS, and HETS monolayers, respectively. These values are in agreement with the general expression for the molecule length obtained by Wasserman et al.[38] for a methyl-terminated monolayer containing $n$ methylene units [SiCl$_3$-(CH$_2$)$_n$-CH$_3$]: $d_{SAM}$ (Å) $= 1.26n + 4.78$. This relation was determined for methyl-terminated monolayers, whereas our monolayers were vinyl-terminated, but the length difference between these two end groups is very low (less than 0.2 Å).[57] The OTS monolayer thickness is equal to $26 \pm 2$ Å, in perfect agreement with the above relation and previous results.[3,38]

**III.3. FTIR Spectroscopy.** For alkylsilane monolayers, the frequency and width of the C−H stretching bands are indicative of the degree of order of the alkyl chains within the monolayers.[3]

**TABLE 2: Thicknesses Measured by Ellipsometry for the Different Alkyl Chain Lengths (HETS, TETS, UETs, and OETS) and the Different π End Groups**

| | HETS | | TETS | | UETS | | OETS | |
|---|---|---|---|---|---|---|---|---|
| | meas (Å) | calc (Å) | meas (Å) | calc (Å) | meas (Å) | calc (Å) | meas (Å) | calc (Å) |
| vinyl | 25.8 | 25.0 | 18.0 | 21.2 | 17.4 | 15.9 | 12.0 | 12.2 |
| COOH | 24.6 | 23.8 | 18.2 | 20.0 | 16.7 | 15.7 | 11.0 | 12.0 |
| phenyl | 31.8 | 28.9 | 21.6 | 25.2 | 20.5 | 20.8 | 19.0 | 17.2 |
| thiophene | 30.0 | 28.2 | 23.0 | 24.5 | 24.7 | 20.1 | 14.5 | 16.9 |
| anthracene | 30.2 | 29.3 | | | | | | |
| pyrene | 31.2 | 32.3 | 26.5 | 28.6 | | | | |
| EDBM | 29.5 | 31.8 | | | | | | |
| EDTM | 27.8 | 31.3 | | | | | | |
| 3T | | | | | 30.1 | 31.7 | 28.0 | 28.0 |
| 4T | | | | | 29.7 | 36.2 | 33.0 | 32.5 |

[a] Measured values (meas) are compared with the calculated length (calc) of the molecule (PM3 calculations). Error is ±2 Å for all measurements.
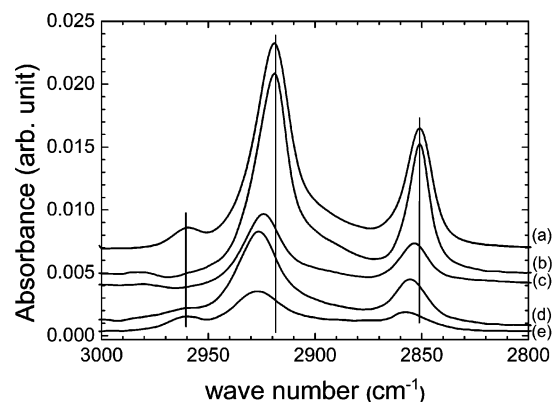
**Figure 5.** ATR-FTIR spectra in the C–H region obtained on a monolayers of (a) OTS, (b) HETS, (c) TETS, (d) UETS, and (e) OETS. The intensities are given in transmission absorbance units. The vertical lines at 2960, 2918, and 2850 cm⁻¹ are provided as guides to the eye.

**Figure 6.** ATR-FTIR spectra in the C=C and C=O regions obtained on (a) vinyl-, (b) COOH-, and (c) anthracene-terminated monolayers. Here, we present an HETS monolayer functionalized by anthracene as an example. The vertical lines are provided as guides to the eye.

The CH₂ vibration peaks for the reference OTS monolayer and the precursor HETS monolayer are $\nu_a = 2918 \pm 1$ cm⁻¹ (antisymmetric) and $\nu_s = 2850 \pm 1$ cm⁻¹ (symmetric) (Figure 5 and Table 3). These values are the fingerprints of a dense and well-ordered monolayer.[3,12,14,15] The positions of these peaks are quite similar to those of CH₃-terminated chains (OTS) used as a reference. We inferred from these values that the alkyl chains in these SAMs are in their all-trans conformation, nearly perpendicular to the substrate (tilt angle of <10°), as expected for a densely packed molecular architecture in the SAM. Amplitudes (areas) of these peaks scale linearly with chain length.

For the monolayers with shorter alkyl chains, the peaks shift to higher wavenumbers (Figure 5 and Table 3). For example, in the case of the OETS monolayer, the peak positions are 2927 and 2858 cm⁻¹ for the antisymmetric and symmetric modes, respectively. Such behavior has also been observed in the case of alkylthiol grafted on gold[3] or platinum[58] substrates. These peak shifts are due to a decrease in the van der Waals interactions between neighboring molecules (which increase with the length of the alkyl chain), leading to an increase in the disorder in the monolayer when the chains are shorter.

The C–H peak positions (symmetric and antisymmetric) after oxidation (i.e., for the COOH-terminated SAM) and after esterification (with the π group) are the same as for the starting vinyl-terminated SAMs (Table 3). The peak amplitude and width are also not changed by these successive chemical processes. We conclude that the chemical functionalization of the starting vinyl-terminated SAMs by oxidation and esterification with the aromatic moieties does not degrade the molecular organization of the alkyl chains in the monolayers.
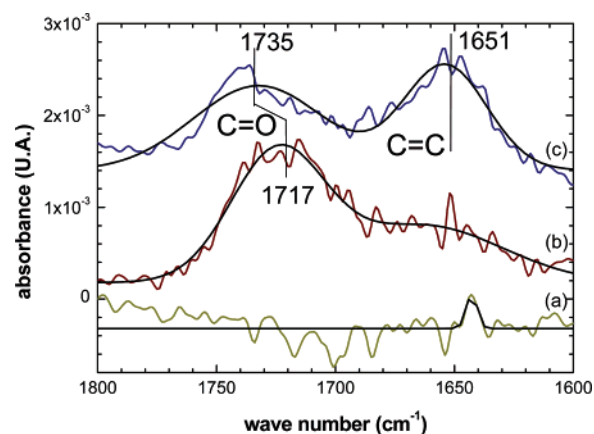
In the region of π bonds, we observed the C=O stretching vibration at 1717 cm⁻¹ (Figure 6) corresponding to the C=O bond in a COOH group.[59] After esterification with aromatic moieties, the stretching C=O mode shifts to 1735 cm⁻¹. This higher value is in agreement with literature values for the C=O vibration mode in an ester bond.[59] In addition, the C=C stretching band at ~1651 cm⁻¹ is clearly observed after esterification, which indicates that the aromatic moieties are effectively attached to the previously formed SAMs.

**III.4. AFM.** Figure 7 shows typical AFM images for the bare substrate, the HETS SAM, and the same HETS SAM functionalized with pyrene groups. Both SAMs are homogeneous; we did not observe holes (at the resolution of the AFM, which is a few tens of nanometers). However, the rms roughness increases, especially after the grafting of the pyrene group. We found rms roughness values of ~0.11 nm for the bare substrate, ~0.16 nm for the HETS SAM, and ~0.22 nm for the HETS–pyrene SAM. This increase might be due to the larger size of the pyrene compared to the alkyl chain and/or to a more disordered organization of the pyrene groups than of the alkyl groups. Note that both SAMs (HETS and HETS–pyrene) display some hollows (darker areas) with a depth of about 0.5–0.7 nm. These "defects" can explain the dispersion observed in the amplitude of the current–voltage curves and the fact that a fraction of the alkyl SAMs were short-circuited (~30%) and that a fraction of the alkyl π-group SAMs showed a weak rectification ratio (<2) or no rectification at all (see below for details and ref 27).
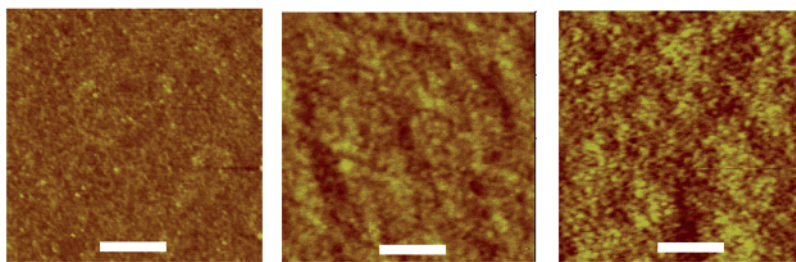
**Figure 7.** Typical AFM images (1 $\mu$m $\times$ 1 $\mu$m) for the bare substrate (left), HETS SAM (middle), and HETS−pyrene SAM (right). The scale bar is 250 nm.

**TABLE 3: Peak Positions of the Symmetric ($\nu_s$) and the Antisymmetric ($\nu_{as}$) C−H Stretching Bands for the Different Monolayers**

| | vinyl-terminated monolayer | | COOH-terminated monolayer | | $\pi$-terminated monolayer | |
|---|---|---|---|---|---|---|
| | $\nu_{as}$ (cm$^{-1}$) | $\nu_s$ (cm$^{-1}$) | $\nu_{as}$ (cm$^{-1}$) | $\nu_s$ (cm$^{-1}$) | $\nu_{as}$ (cm$^{-1}$) | $\nu_s$ (cm$^{-1}$) |
| OTS | 2918 ± 1 | 2850 ± 1 | | | | |
| HETS | 2918 ± 1 | 2850 ± 1 | 2918 ± 1 | 2850 ± 1 | 2918 ± 1 | 2850 ± 1 |
| TETS | 2924 ± 1 | 2853 ± 1 | 2924 ± 1 | 2853 ± 1 | 2924 ± 1 | 2853 ± 1 |
| UETS | 2926 ± 1 | 2856 ± 1 | 2926 ± 1 | 2856 ± 1 | 2926 ± 1 | 2856 ± 1 |
| OETS | 2927 ± 1 | 2858 ± 1 | 2927 ± 1 | 2858 ± 1 | 2927 ± 1 | 2858 ± 1 |

**TABLE 4: Summary of the Capacitance Measured at 1 MHz for the Different Monolayers[a]**

| monolayer | $C_{SAM}$ ($\mu$F/cm$^2$) | $\epsilon_{SAM}$ | $n$ | $d_{SAM}$ (Å) | $d_{th}$ (Å) |
|---|---|---|---|---|---|
| TETS/phenyl | 1.00 ± 0.20 | 2.25 ± 0.02 | 1.5 ± 0.1 | 21 ± 3 | 25 |
| TETS/thiophene | 1.00 ± 0.50 | 2.35 ± 0.03 | 1.5 ± 0.3 | 22 ± 3 | 25 |
| TETS/pyrene | 1.10 ± 0.70 | 2.75 ± 0.09 | 1.7 ± 0.5 | 23 ± 3 | 28 |
| HETS | 0.80 ± 0.10 | 2.33 ± 0.04 | 1.5 ± 0.2 | 25 ± 2 | 25 |
| HETS/phenyl | 0.66 ± 0.04 | 2.30 ± 0.03 | 1.5 ± 0.2 | 31 ± 2 | 29 |
| HETS/thiophene | 0.66 ± 0.02 | 2.21 ± 0.02 | 1.5 ± 0.1 | 30 ± 2 | 28 |
| HETS/anthracene | 0.94 ± 0.01 | 2.80 ± 0.01 | 1.7 ± 0.1 | 27 ± 3 | 29 |
| HETS/pyrene | 0.59 ± 0.09 | 2.10 ± 0.05 | 1.5 ± 0.2 | 32 ± 2 | 32 |
| HETS/EDBM | 0.61 ± 0.03 | 2.06 ± 0.02 | 1.4 ± 0.2 | 31 ± 3 | 32 |
| HETS/EDTM | 0.77 ± 0.01 | 2.32 ± 0.01 | 1.5 ± 0.1 | 27 ± 3 | 31 |
| OTS | 1.06 ± 0.05 | 2.7 ± 0.03 | 1.6 ± 0.1 | 22 ± 2 | 26 |

[a] Taking into account the oxide capacitance and the Debye capacitance of the semiconductor, we deduced the capacitance of the monolayer. Coupling these measurements with ellipsometry (from Table 2) gave us the dielectric constant and the thickness of the monolayers (see text or details).

## IV. Electrical Properties

**IV.1. Capacitance Measurements.** To determine the impact of the $\pi$ group on the dielectric permittivity, we measured the capacitance of the monolayers. Capacitance can change for two reasons: (i) an increase in thickness and (ii) a change in the dielectric permittivity when anchoring $\pi$ moieties with a dipole moment higher than that of the pure alkyl chain (almost nonpolar). Combining capacitance and ellipsometry measurements (see section 2.4) allows us to determine both the dielectric constant and the thickness of the end-group-functionalized SAMs. From the capacitance measurements, we can extract the ratio $\epsilon_{SAM}/d_{SAM}$, where $\epsilon_{SAM}$ is the SAM dielectric constant and $d_{SAM}$ is the SAM thickness, and from the ellipsometry, we can extract the product $nd_{SAM}$, where $n$ is the optical refraction index and $d_{SAM}$ is as above. Assuming that $\epsilon_{SAM} = n^2$, we combined the two results to calculate $\epsilon_{SAM}$, $n$, and $d_{SAM}$ (Table 4). The refractive index ($n$) values for all of the monolayers are around 1.5. Similar values of $n$ for both alkyl and alkyl-$\pi$ SAMs are expected because the $\pi$ groups are not highly polar. This result confirms the choice of 1.5 for the refractive index made in section 2.4 for the ellipsometry measurements and the similar values of $\epsilon$ for the alkyl chain and the $\pi$ group in eq 3 (see below). The thicknesses deduced by combining ellipsometry and capacitance measurements are in agreement with the expected values and with the thicknesses measured by ellipsometry alone.

**IV.2. Conductivity Measurements.** Figure 8 shows typical current density vs voltage curves ($J$−$V$) for several $\pi$-terminated SAMs made with HETS (Figure 8a and b) and OETS (Figure 8c) as the alkyl spacer. The $J$−$V$ curves for alkylsilane SAMs (without $\pi$ groups) are taken as the reference (Figure 8d). The $J$−$V$ curves for the CH$_3$-terminated (OTS) and vinyl-terminated (OETS, TETS, and HETS) SAMs are symmetric (see Figure 8d, for the case of OTS). We also verified that the introduction of the polar ester group is not responsible for the rectification behavior of the $\pi$-terminated SAMs. Figure 8d shows the $J$−$V$ curve for the COOH-terminated SAM (as obtained after step 1 described above and based on a pristine HETS SAM). In the COOH-terminated case, the shape of the $J$−$V$ plot is less linear, and a small asymmetry is observed with a slightly higher current at positive bias (a ratio ∼1.35 at |1 V|), i.e., opposite to the case of $\pi$-terminated SAMs. In all other cases, with the $\pi$ moieties at the end, we observed a rectification behavior, i.e., a higher current density at −1 V than at 1 V. To further analyze this rectification effect, we compared the dispersion for the current densities at −1 and 1 V (see the example for HETS/phenyl in Figure 9). The observed distributions were fitted by two Gaussian curves that are not at the same position; the current density at −1 V is shifted to higher values (by almost a factor 10 in that case). This statistical analysis clearly reveals the rectification behavior despite the inherent current dispersion already observed with these SAMs. The electrical properties for all of the monolayers studied in this work are reported in Table 5. For every $\pi$-functionalized monolayer, we define a rectification ratio (RR) equal to the average current density at −1 V (in absolute value) divided by the average current density at 1 V (RR = $|J_{-1 V}|/J_{1 V}$). The average values of RR are in the range between 3 and 13 (Table 5) for the functionalized monolayers, with the highest RR value of 37 for the OETS/thiophene monolayer. We did not observe a significant variation of RR with the chemical nature of the end groups, nor did we observe any correlation with the alkyl spacer length (the sample-to-sample variations of the RR values were too large, with relative scattering of about 50% for a given end group and alkyl chain length).

Figure 10 is a schematic representation of the energy diagram of the silicon (covered by native SiO$_2$)/alkyl $\pi$ group/metal
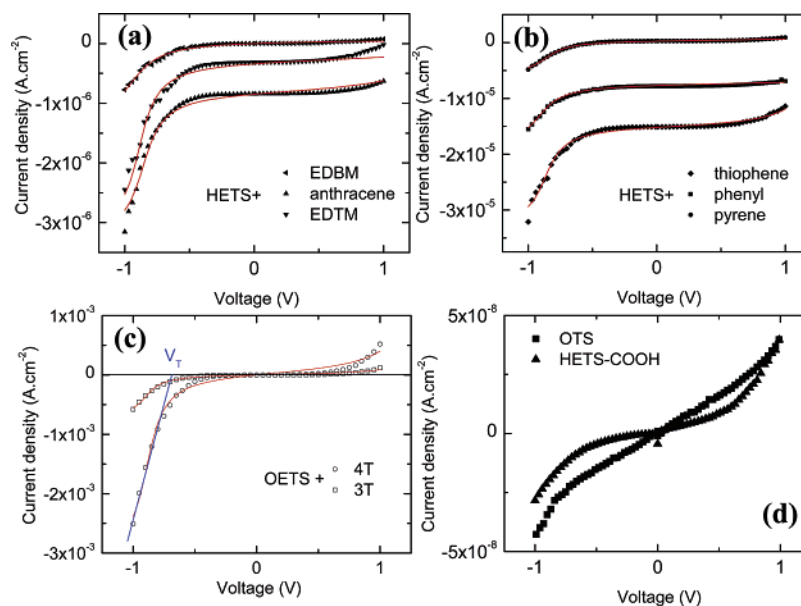
**Figure 8.** Typical current density−voltage characteristics of the Si/σ−π/Al junctions: (a) HETS/EDBM (solid, left-facing triangle), HETS/anthracene (▲), HETS/EDTM (▼) (b) HETS/phenyl (■), HETS/pyrene (●), HETS/thiophene (◆); and (c) OETS/3T (□), OETS/4T (○). Some curves are vertically shifted for clarity. Red solid lines are fits with eq 2. For OETS/4T, we show the determination of the threshold voltage for rectification, $V_T$, which is defined as the intercept between a linear fit (dotted line) of the current at high negative voltages and the x axis. (d) Current−voltage characteristics for OTS and COOH-terminated HETS (i.e., without π end group) are presented as references.
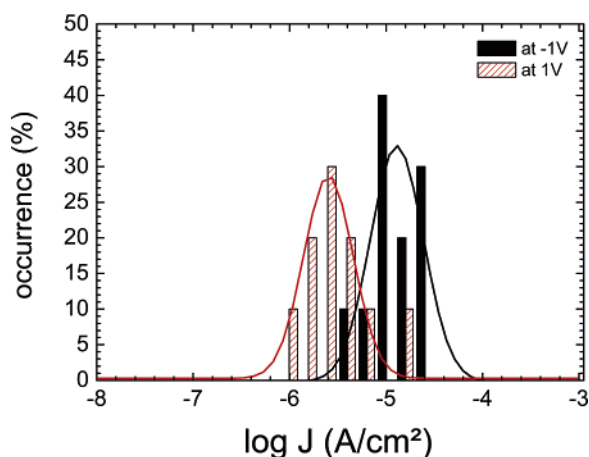


**Figure 9.** Example of the dispersion of the current density for the HETS/phenyl SAM (10 measured samples). We compare the dispersion for the current densities of −1 and 1 V. For each monolayer, the center of the Gaussian and the fwhm (full width at half-maximum) give the average value and the statistical dispersion, respectively, for the current density.

junction: (a) at 0 V and (b) at a negative bias on the metal electrode for which a resonant electron transfer can occur through the π level from the metal to the empty states of the Si conduction band (CB). We have $W_M \approx 4.2$ eV for Al and $W_{Si} \approx \chi_{Si} = 4.1$ eV for n⁺-type Si, where $\chi_{Si}$ is the electron affinity. σ, π and σ*, π* are the HOMO and LUMO of the alkyl chain and π group, respectively. σ* is about 4.2 eV above the Si CB, and σ is about 4.2 eV below the Si valence band (VB).[19,27] The positions of the CB and VB of the ultrathin (∼1 nm) native SiO₂ are not given precisely, but they are likely below the LUMO and HOMO, respectively, of the alkyl chain. For instance, values as low as ∼1 eV have been reported for the CB of such an ultrathin native oxide (see compiled data in Figure 3 of ref 60). The positions of the π and π* levels and $E_0$ should depend on the nature of the π groups. We also notice that the role played by the native oxide as a tunnel barrier is negligible (at first order) compared to that of the alkyl-chain monolayer.

Comparing the current densities in Al/Si, Al/native SiO₂/Si, Al/C18/Si, and Al/C18/native SiO₂/Si (where C18 stands for a monolayer of an 18-carbon-atom alkyl chain), we measured[18,60,61] (at 0.5 V) values of ∼10², ∼50, and ∼10⁻⁷−10⁻⁸ A/cm² (for the latter two junctions), respectively. This justifies the neglect of the native oxide in analyzing the J−V curves of the present devices. The rectification behavior of these σ−π SAMs is due to the resonant tunneling through one of the MOs of the π group (Figure 10) resulting from geometrical asymmetry (the π group is closer to the metal electrode than the silicon) and the energy asymmetry in the positions of the MOs with respect to the Fermi level of the electrodes.[62,63] The rectification effect arises when a negative bias is applied on the Al electrode because the energy difference between the silicon Fermi energy (pinned at the conduction band, CB, for the degenerate Si) and the HOMO (π orbital) is lower than the LUMO (π* orbital). If we assume that the π end group is almost at the Al electrode potential (given that this group is in close contact with the electrode) and that a large part of the potential drop takes place in the alkyl chains, the threshold (in absolute value) required to have a resonance is lower for a negative bias than for a positive bias. As a consequence, the J−V curves can be fitted by a one-level model in which the conduction is dominated by charge transport through a single energy level located at a position $E_0$ ($E_0 < 0$) below the electrode Fermi energy. This allows an experimental determination of the energy position. The current density is given by[64,65]

$$J = \frac{2J_0}{\pi}\{\tan^{-1}[\theta(|E_0| + \eta eV)] - \tan^{-1}[\theta(|E_0| - (1-\eta)eV)]\} \quad (2)$$

where V is the applied potential on the metal electrode (Si is grounded), e is the electron charge, η is the fraction of the potential across the π moiety, $J_0$ is the saturation current, and θ is an electrode/molecule coupling parameter. The η value was estimated using a simple dielectric model where the σ and π parts of the SAM have thicknesses of $d_\sigma$ and $d_\pi$ and dielectric

Electron Transport through Rectifying SAM Diodes on Si

*J. Phys. Chem. B, Vol. 110, No. 28, 2006* **13955**

**TABLE 5: Average Rectification Ratio [RR = |J(−1 V)|/J(+1 V)], Saturation Current Density ($J_0$), Experimental Position of the HOMO Level ($E_0$) with Respect to the Si CB,[a] Coupling Parameter ($\theta$), Theoretical HOMO in a Vacuum (PM3 Calculations),[a] Gas-Phase Ionization Potential ($I_P$, eV),[a] and Molecular Diode Threshold Voltage for the Various $\pi$ End Groups**

| $\pi$ group | RR | $J_0$ (A cm$^{-2}$) | $E_0$ (eV) | $\theta$ (eV$^{-1}$) | HOMO PM3 (eV) | $I_P$ (eV) | $V_T$ (V) |
|---|---|---|---|---|---|---|---|
| benzene | 4.8 ± 3.3[b] | 1.3 × 10$^{-5}$ | −0.82 ± 0.16 | 5.0 ± 2.9 | −5.65 | −5.1[87] | −0.64 ± 0.07 |
| thiophene | 13.3 ± 13[c] | 3.3 × 10$^{-4}$ | −0.80 ± 0.14 | 7.5 ± 2.8 | −5.44 | −4.7[87] | −0.65 ± 0.07 |
|  | 2.7 ± 1.4[b] | 1.8 × 10$^{-5}$ |  |  |  |  |  |
| EDBM | 4.7 ± 2.9[b] | 7.8 × 10$^{-5}$ | −0.75 ± 0.03 | 8.5 ± 0.5 | −4.92 | −3.6[88] | −0.68 ± 0.01 |
| EDTM | 6.7 ± 2[b] | 6.6 × 10$^{-6}$ | −0.73 ± 0.03 | 7.4 ± 2.7 | −4.88 | −4.2[88] | −0.68 ± 0.04 |
| pyrene | 9.4 ± 3.8[b] | 9.1 × 10$^{-6}$ | −0.71 ± 0.04 | 10.1 ± 1.5 | −4.15 | −3.45[87] | −0.68 ± 0.02 |
| anthracene | 8.1 ± 2.9[b] | 9.4 × 10$^{-6}$ | −0.75 ± 0.09 | 10.4 ± 1.2 | −4.15 | −3.25[87] | −0.7 ± 0.02 |
| 3T | 3.6 ± 1.4[c] | 4.7 × 10$^{-3}$ | −0.81 ± 0.1 | 8.6 ± 1.6 | −4.58 | −3.3[89] | −0.68 ± 0.05 |
| 4T | 4.6 ± 0.2[c] | 9.4 × 10$^{-3}$ | −0.77 ± 0.07 | 9.2 ± 0.3 | −4.56 | −3.18[89] | −0.7 ± 0.02 |

[a] In all cases, the energy reference is taken at the Si CB. We subtracted the Si work function, $W_{Si}$ = 4.1 eV, from the HOMO PM3, and the gas-phase which are usually referenced to the vacuum level. [b] Alkyl chain = HETS  [c] Alkyl chain = OETS.
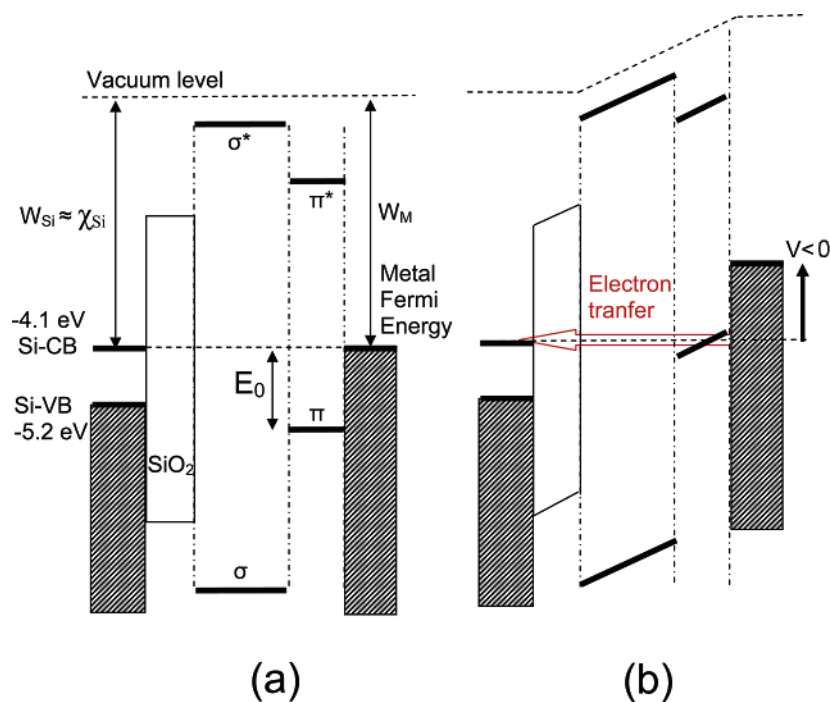


**Figure 10.** Schematic representation of the energy diagram of the silicon (covered by native SiO$_2$)/alkyl $\pi$ group/metal junction: (a) at 0 V and (b) at a negative bias on the metal electrode for which resonant electron transfer can occur through the $\pi$ level from the metal to the empty states of the Si CB. For simplicity, we assumed a linear potential drop through the SAM.

constants of $\epsilon_\sigma$ and $\epsilon_\pi$, respectively[62,66]

$$\eta = 1 - \frac{1}{2}\frac{1}{1 + \dfrac{\epsilon_\pi d_\sigma}{\epsilon_\sigma d_\pi}} \quad (3)$$

In practice, the dielectric constants of the $\pi$ groups used in this work and the alkyl chains are almost the same (see next section),[67] so eq 3 reduces to $\eta = (d_\sigma + 0.5d_\pi)/(d_\sigma + d_\pi)$, which simply represents the relative position of the center of gravity of the $\pi$ moiety measured from the Si substrate. Taking the thicknesses derived from the ellipsometry measurements of the SAM before and after esterification of the $\pi$ end group (see section 3.2), typical values of ∼0.83, ∼0.87, and ∼0.9 were obtained for the SAMs based on OETS, TETS, and HETS, respectively. As shown in Figure 8, the measured J−V curves can be satisfactorily adjusted with this equation ($R^2 \geq 0.97$). The solid lines in Figure 8 are the best fits obtained with these equations, and the values of the adjustable parameters $J_0$, $E_0$, and $\theta$ are given in Table 5. We then investigated a relationship between the intrinsic electronic structure of the $\pi$ group (their

MOs in a vacuum), the electronic structure of the Si/$\sigma$−$\pi$/metal junction (MOs of the $\pi$ group embedded in the junction), and the MRJ experimental behavior. For this, we compared the HOMO energy of the $\pi$ group in a vacuum (PM3 calculation), the HOMO energy of the $\pi$ group as deduced from the gas-phase ionization potential, and the experimental HOMO position in the junction with respect to the silicon Fermi energy (i.e., $E_0$ deduced from the fit of the analytical current density equation as shown above). These values are compared in Table 5 and Figure 11. It is clear that the experimentally determined HOMO level of the $\pi$ groups in the MRJ markedly differs from the single-molecule values (both PM3 and IP). As explained in the Introduction, there are many reasons for these differences: molecule/surface interactions leading to charge transfer and interface dipole formation, polarization energy in the solid state that moves the HOMO (LUMO) upward (downward) with respect to the gas-phase value, or an intrinsic dipole of the molecule itself. For instance, PM3 calculations show that all of the molecules used in this work have a dipole moment of about 2−4 D along their long axis, with the positive charge at the Si side and the negative charge at the ester side. As a consequence,
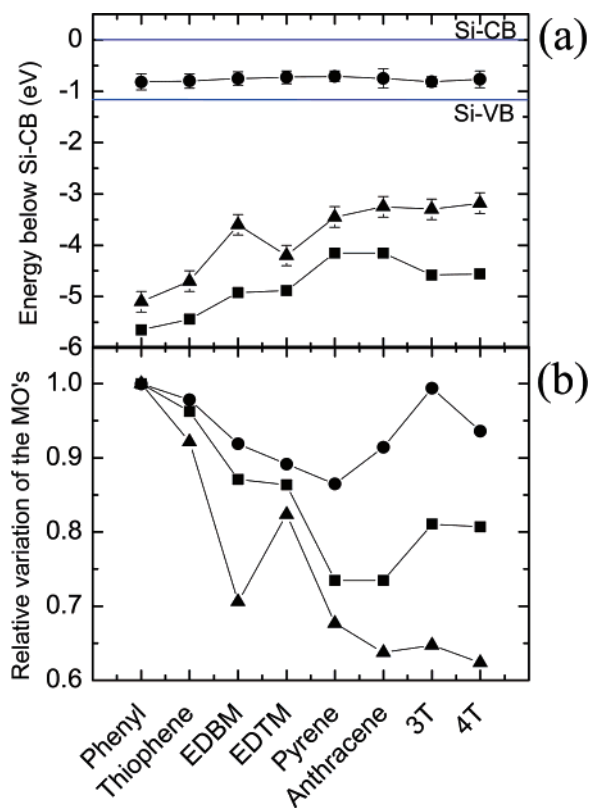
**Figure 11.** (a) Energy position (with respect to the Si CB) for the different $\pi$ groups: ($\bullet$) chemisorbed SAM on Si as determined from the present experiments, ($\blacksquare$) PM3 calculations for a single molecule in a vacuum, and ($\blacktriangle$) experimental gas-phase ionization potential (see references in Table 5). (b) Same data normalized to the corresponding value for the phenyl group.

this dipole shifts the MOs of the $\pi$ group upward by a quantity $\Phi = \mu_D/\epsilon A_{mol}$ (assuming the molecules have their long axis normal to the surface), where $\mu_D$ is the moment of the molecule, $\epsilon$ is the dielectric constant, and $A_{mol}$ is the area per molecule. Assuming a relative dielectric constant of 3 and an average $A_{mol}$ value of 30−50 Å$^2$ (depending on the molecule), we get $\Phi$ in the range of 1−2 eV. These values are consistent with several experimental determinations for SAMs on both metal and Si surfaces,[68,69] but are not sufficient to explain the observed differences. More detailed calculations (both ab initio and semiempirical) to determine the full electronic structure of the Si/$\sigma$−$\pi$/metal junctions are in progress and will be reported elsewhere.[70] A striking experimental feature is that the HOMO energy positions in the MRJ are almost the same regardless of the $\pi$ molecules. They vary from 0.71 to 0.82 eV below the Si conduction band (Figure 11a), or in other words, the metal Fermi energy level is pinned about 0.71−0.82 eV above the $\pi$ HOMO. This is a very small variation compared to what was expected, ∼1.5 eV, from the gas-phase ionization and PM3 levels (Figure 11a). However, plotting the HOMO levels arbitrarily normalized to the level for the phenyl end group (Figure 11b), we show that the relative trends for the variations of the HOMO levels versus the nature of the $\pi$ groups are conserved in the molecular junction, the amplitude of these variations being screened in the junction. This behavior is the fingerprint of Fermi-level pinning at the metal/molecule interface. A typical way to quantify Fermi-level pinning consists of calculating the so-called interface slope parameter, $S = |dE_F/dW_M|$, where $W_M$ is the metal work function and $E_F$ is the position of the Fermi level with respect to one of the molecular orbitals. Here, because we used only one metal and various organic molecules, one can
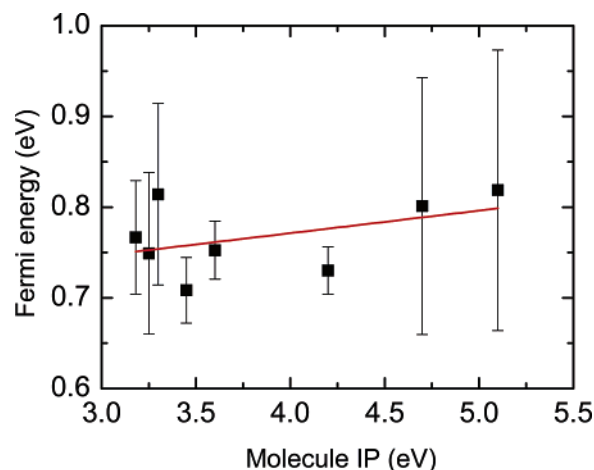


**Figure 12.** Metal Fermi energy position (with respect to the HOMO of the $\pi$ group) versus the gas-phase $I_P$ of the $\pi$ groups (data from Table 5 and Figure 11a). The plotted values correspond to −$E_0$, where $E_0$ was determined from the fit of eq 2 on the $J$−$V$ curves. The gas-phase $I_P$ is the absolute value with respect to Si CB level. The line is a linear fit with a slope of ∼0.025 ± 0.02.

equivalently determine $S = |dE_F/dI_P|$, where $I_P$ is the ionization potential of the molecule. $S = 1$ corresponds to the Schottky−Mott model,[71,72] and $S = 0$ corresponds to the Bardeen[73] model. In the former case, the energetics of the interface is strictly dictated by the difference in the work function of the two materials, whereas the latter case assumes that a high density of interface states pins the position of the Fermi level regardless of the nature of the metal electrode. From the plot of $E_F$ vs $I_P$ (Figure 12), we deduced an average slope of $S = 0.025 ± 0.02$. This slope is related to the density of metal/organic interface states at the Fermi level, $D_{it}(E_F)$, by[74] $D_{it} = [\epsilon_0\epsilon_i(1 − S)]/e\delta S$, where $\epsilon_0$ is the vacuum dielectric constant, $\epsilon_i$ is the dielectric constant of the organic/metal interface region, $\delta$ is its thickness, and $e$ is the electron charge. We do not know the actual interface dipole in our devices,[75] but we can nevertheless try to get an estimate of $D_{it}$. Considering $\delta$ to be about 5 Å and assuming $\epsilon_i \approx 2.5−3$ as in the SAM, we get $D_{it}(E_F)$ in the range of ∼10$^{15}$ cm$^{-2}$ eV$^{-1}$.

A possible origin of the observed metal Fermi pinning is the existence of metal-induced gap states (MIGS)[76] or the creation of chemically induced gap states (CIGS) at the metal/organic interface through the possible reaction of aluminum with the $\pi$-conjugated moieties.[33] Recently, MIGS at metal/organic interfaces have been theoretically and experimentally studied in PTCDA/Au.[76] The creation of MIGS results in a pinning of the metal Fermi level very near the charge neutrality level (CNL), i.e., the energy position for which the total charge integrated over the band-gap density is null. In our case, another likely origin of the metal Fermi pinning is the creation of CIGS at the metal/organic interface through the possible chemical reaction of aluminum with the $\pi$-conjugated moieties.[33] Typical examples of this behavior are the Alq$_3$/Mg and Alq$_3$/Al interfaces.[77,78] The chemical reactivity of vapor-deposited Al on SAMs of alkyl chains bearing various end groups has been widely studied.[79−83] It was shown that Al reacts with oxygen-based terminal groups such as −COOH, −CO$_2$CH$_3$, −OH, and −OCH$_3$ to form organoaluminum complexes. However, reports on vapor deposition of metals on SAMs bearing conjugated end groups are scarce. Ahn and Whitten[84] observed a strong chemical interaction between vapor-deposited Al and a thiophene-terminated SAM that appears as a metal-induced, low-binding-energy component in the S$_{2p}$ and C$_{1s}$ main peaks of X-ray photoemission spectra. Similarly, de Boer and
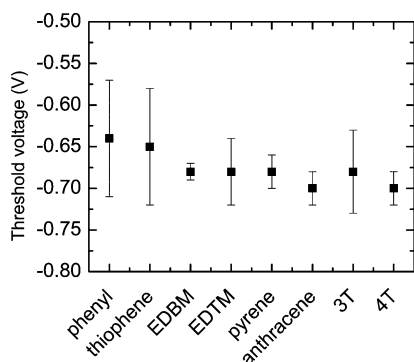
Electron Transport through Rectifying SAM Diodes on Si

*J. Phys. Chem. B, Vol. 110, No. 28, 2006* **13957**



**Figure 13.** Threshold voltage for rectification, $V_T$, as a function of the nature of the $\pi$ end group. $V_T$ is defined as the intercept between a linear fit (dotted line in Figure 8) of the current at high negative voltages and the $x$ axis (see Figure 8). The error bars are the fwhm (full width at half-maximum) of the data statistical distribution obtained on a large number ($>20$) of devices for each $\pi$ group.

co-workers reported (infrared spectroscopy) that Al atoms reacted with the conjugated backbone of thiol-modified oligophenyl SAMs on gold. Thus, it is likely that Al chemically reacts with any of the eight $\pi$ groups used in this work or even with the ester group if some Al atoms penetrate into the SAMs. Detailed theoretical calculations are in progress to determine the electronic structure of the whole Si/molecule/metal junction, which requires an exact treatment of the metal/organic interface dipole.[76,85] Finally, Figure 13 shows the MRJ threshold voltage, $V_T$, which is defined as the intercept between a linear fit of the current at high negative voltages and the $x$ axis. All of these values are summarized in Table 5. As a consequence of the pinning of the Fermi level, $V_T$ is independent of the nature of the $\pi$ group. A negative bias of $V_T \approx -E_0/e\eta$ (i.e., approximately $-E_0/e$ because $\eta \approx 1$; see above) is necessary to line up the HOMO on resonance with the CB of the n$^+$-doped silicon. The actual values $V_T \approx -0.65$ to $-0.7$ V are quite consistent with this explanation. A further improvement would be to chemically tune the rectification behavior of the molecular diode. This requires decoupling the $\pi$ group from the metal electrode, which could be achieved by introducing a short alkyl spacer chain between the $\pi$ group and the top electrode. For instance, it has been calculated that rectification will persist if the ratio of the number of carbon atoms in the lower and upper alkyl spacer chains is larger than 2.[86]

## V. Conclusion

We have demonstrated that SAMs containing $\pi$ groups (phenyl, anthracene, pyrene, ethylene dioxythiophene, ethylene dioxyphenyl, thiophene, terthiophene, and quaterthiophene) can be obtained by sequential grafting of alkyl chains (different chain lengths from 6 to 15 methylene groups) that are functionalized in a second step. Such SAMs are reasonably well structured at the macro- and microscopic scales, as can be seen by contact angle measurements, ellipsometry, IR spectroscopy, and AFM. For all of the $\pi$ groups investigated here, we observed a rectification behavior in their current density vs voltage characteristics, which extends our preliminary work using phenyl and thiophene groups.[27] A simple analytical model was fitted to the experimental current–voltage curves to determine the position of the $\pi$-group molecular orbitals with respect to the electronic structures of the silicon substrate and the metal top electrode. We conclude that Fermi-level pinning at the $\pi$ group/metal interface is mainly responsible for the observed behavior. It also explains why the rectification effect does not depend on the nature of the $\pi$ groups, even though they were chosen to

have significant variations in their electronic molecular orbitals in a vacuum.

## References and Notes

(1) ITRS. *International Technology Roadmap for Semiconductors*, 2005.

(2) Compano, R.; Molenkamp, L.; Paul, D. J. Technology roadmap for nanoelectronics; European Commission, IST Programme, Future and Emerging Technologies, 2000.

(3) Ulman, A. *An Introduction to Ultrathin Organic Films: From Langmuir–Blodgett to Self-Assembly*; Academic Press: Boston, 1991.

(4) Schreiber, F. *Prog. Surf. Sci.* **2000**, *65*, 151−256.

(5) Love, J. C.; Estroff, L. A.; Kriebel, J. K.; Nuzzo, R. G.; Whitesides, G. M. *Chem. Rev.* **2005**, *105*, 1103−1169.

(6) Bruening, M.; Moons, E.; Yaron-Marcovitch, D.; Cahen, D.; Libman, J.; Shanzer, A. *J. Am. Chem. Soc.* **1994**, *116*, 2972−2977.

(7) Cohen, R.; Bastide, S.; Cahen, D.; Libman, J.; Shanzer, A.; Rosenwaks, Y. *Opt. Mater.* **1998**, *9*, 394−400.

(8) Cohen, R.; Zenou, N.; Cahen, D.; Yitzchaik, S. *Chem. Phys. Lett.* **1997**, *279*, 270−274.

(9) Joachim, C.; Gimzewski, J. K.; Aviram, A. *Nature* **2000**, *408*, 541−548.

(10) Bigelow, W. C.; Pickett, D. L.; Zisman, W. A. *J. Colloid Sci.* **1946**, *1*, 513−538.

(11) Maoz, R.; Sagiv, J. *J. Colloid Interface Sci.* **1984**, *100*, 465−496.

(12) Brzoska, J. B.; Shahidzadeh, N.; Rondelez, F. *Nature* **1992**, *360*, 719−721.

(13) Brzoska, J. B.; Ben Azouz, I.; Rondelez, F. *Langmuir* **1994**, *10*, 4367−4373.

(14) Allara, D. L.; Parikh, A. N.; Rondelez, F. *Langmuir* **1995**, *11*, 2357−2360.

(15) Parikh, A. N.; Allara, D. L.; Ben Azouz, I.; Rondelez, F. *J. Phys. Chem.* **1994**, *98*, 7577−7590.

(16) Mann, B.; Kuhn, H. *J. Appl. Phys.* **1971**, *42*, 4398−4405.

(17) Polymeropoulos, E. E.; Sagiv, J. *J. Chem. Phys.* **1978**, *69*, 1836−1847.

(18) Boulas, C.; Davidovits, J. V.; Rondelez, F.; Vuillaume, D. *Phys. Rev. Lett.* **1996**, *76*, 4797−4800.

(19) Vuillaume, D.; Boulas, C.; Collet, J.; Allan, G.; Delerue, C. *Phys. Rev. B* **1998**, *58*, 16491−16498.

(20) Collet, J.; Tharaud, O.; Chapoton, A.; Vuillaume, D. *Appl. Phys. Lett.* **2000**, *76*, 1941−1943.

(21) Collet, J.; Vuillaume, D. *Appl. Phys. Lett.* **1998**, *73*, 2681−2683.

(22) Halik, M.; Klauk, H.; Zschieschang, U.; Schmid, G.; Dehm, C.; Schütz, M.; Maisch, S.; Effenberger, F.; Brunnbauer, M.; Stellacci, F. *Nature* **2004**, *431*, 963−966.

(23) Roth, K. M.; Lindsey, J. S.; Bocian, D. F.; Kuhr, W. G. *Langmuir* **2002**, *18*, 4030−4040.

(24) Roth, K. M.; Yasseri, A. A.; Liu, Z.; Dabke, R. B.; Malinovskii, V.; Schweikart, K.-H.; Yu, L.; Tiznado, H.; Zaera, F.; Lindsey, J. S.; Kuhr, W. G.; Bocian, D. F. *J. Am. Chem. Soc.* **2003**, *125*, 505−517.

(25) Kuhr, W. G.; Gallo, A. R.; Manning, R. W.; Rhodine, C. W. *Mater. Res. Soc. Bull.* **2004**, *29*, 838−842.

(26) Guisinger, N. P.; Greene, M. E.; Basu, R.; Baluch, A. S.; Hersam, M. C. *Nano Lett.* **2004**, *4*, 55−59.

(27) Lenfant, S.; Krzeminski, C.; Delerue, C.; Allan, G.; Vuillaume, D. *Nano Lett.* **2003**, *3*, 741−746.

(28) Xue, Y.; Datta, S.; Ratner, M. A. *J. Chem. Phys.* **2001**, *115*, 4292−4299.

(29) Tomfohr, J. K.; Sankey, O. F. *Phys. Rev. B* **2002**, *65*, 245105.

(30) Yaliraki, S. N.; Roitberg, A. E.; Gonzalez, C.; Mujica, V.; Ratner, M. A. *J. Chem. Phys.* **1999**, *111*, 6997−7002.

(31) Tian, W.; Datta, S.; Hong, S.; Reifenberger, R.; Henderson, J. I.; Kubiak, C. P. *J. Chem. Phys.* **1998**, *109*, 2874−2882.

(32) Vondrak, T.; Cramer, C. J.; Zhu, X.-Y. *J. Phys. Chem. B* **1999**, *103*, 8915−8919.

(33) Kahn, A.; Koch, N.; Gao, W. *J. Polym. Sci. B: Polym. Phys.* **2003**, *41*, 2529−2548.

(34) Ishii, H.; Sugiyama, K.; Ito, E.; Seki, K. *Adv. Mater.* **1999**, *11*, 605−625.

(35) Haick, H.; Ambrico, M.; Ligonzo, T.; Cahen, D. *Adv. Mater.* **2004**, *16*, 2145−2151.

(36) Vilan, A.; Ghabboun, J.; Cahen, D. *J. Phys. Chem. B* **2003**, *107*, 6360−6376.

(37) Vilan, A.; Shanzer, A.; Cahen, D. *Nature* **2000**, *404*, 166.

(38) Wasserman, S. R.; Tao, Y.; Whitesides, G. M. *Langmuir* **1989**, *5*, 1074−1087.

(39) Bonnier, M. Ph.D. Thesis, Université Paris VI, Paris, 1997.

(40) It is our understanding from several years of experience that performing all of these chemical reactions in a well-controlled clean room ambient and with high-quality chemicals (as pure as possible, depending on the quality of the purchased chemicals, we used them as received or after homemade purification) strongly helps in obtaining reliable and reproducible procedures for the SAM synthesis.

(41) Benzyl alcohol (99%) and 3-thiophenemethanol (98%) were purchased from Sigma-Aldrich. These chemicals were used as received.

(42) 9-Anthracenemethanol (97%) and 1-pyrenemethanol (98%) were purchased from Sigma-Aldrich and were used as received.

(43) MacEachern, A.; Soucy, C.; Leitch, L. C.; Arnason, J. T.; Morand, P. *Tetrahedron* **1988**, *44*, 2403.

(44) Blohm, M. L.; Pickett, J. E.; Vandort, P. C. U.S. Patent 5,111,327, 1992.

(45) Pei, Q.; Zucharello, G.; Ahlskog, M.; Inganäs, O. *Polymer* **1994**, *35*, 1347.

(46) Lima, A.; Schottland, P.; Sadki, S.; Chevrot, C. *Synth. Met.* **1998**, *93*, 33−41.

(47) Vuillaume, D. In *Amorphous and Crystalline Insulating Thin Films*; Warren, W. L., Devine, R. A. B., Matsumura, M., Cristoloveanu, S., Homma, Y., Kanicki, J., Eds.; Materials Research Society: Boston, 1997; Vol. 446, pp 79−90.

(48) Simmons, J. G. *J. Appl. Phys.* **1963**, *34*, 2581−2590.

(49) Zhou, C.; Deshpande, M. R.; Reed, M. A.; Jones, L., II; Tour, J. M. *Appl. Phys. Lett.* **1997**, *71*, 611−613.

(50) Steel, A. B.; Cheek, B. J.; Miller, C. J. *Langmuir* **1998**, *14*, 5479−5486.

(51) Israelachvili, J. *Intermolecular and Surface Forces*, 2nd ed.; Academic Press: New York, 1991.

(52) Bain, C. D.; Evall, J.; Whitesides, G. M. *J. Am. Chem. Soc.* **1989**, *111*, 7155−7164.

(53) Cassie, A. B. D.; Baxter, S. *Trans. Faraday Soc.* **1944**, *3*, 11.

(54) Appelhans, D.; Ferse, D.; Adler, H.-J. P.; Plieth, W.; Fikus, A.; Grundke, K.; Schmitt, F.-J.; Bayer, T.; Adolphi, B. *Colloids Surf. A* **2000**, *161*, 203-212.

(55) Zisman, W. In *Contact Angle, Wettability, and Adhesion*; Fowkes, F. M., Ed.; American Chemical Society: Washington, DC, 1964; Vol. 43, pp 1−51.

(56) CambridgeSoft Corporation: Cambridge, U.K., 1996.

(57) Lyde, D. R., Ed. *Handbook of Chemistry and Physics*, 74th ed.; CRC Press: Boca Raton, FL, 1993−1994.

(58) Li, Z.; Chang, S.-C.; Williams, R. S. *Langmuir* **2003**, *19*, 6744−6749.

(59) Maoz, R.; Sagiv, J.; Degenhardt, D.; Möhwald, H.; Quint, P. *Supramol. Sci.* **1995**, *2*, 9−24.

(60) Vuillaume, D.; Boulas, C.; Collet, J.; Davidovits, J. V.; Rondelez, F. *Appl. Phys. Lett.* **1996**, *69*, 1646−1648.

(61) Miramond, C.; Vuillaume, D. *J. Appl. Phys.* **2004**, *96*, 1529−1536.

(62) Krzeminski, C.; Allan, G.; Delerue, C.; Vuillaume, D.; Metzger, R. M. *Phys. Rev. B* **2001**, *64*, 085405.

(63) Datta, S.; Tian, W.; Hong, S.; Reifenberger, R.; Henderson, J. I.; Kubiak, C. P. *Phys. Rev. Lett.* **1997**, *79*, 2530−2533.

(64) Peterson, I. R.; Vuillaume, D.; Metzger, R. M. *J. Phys. Chem. A* **2001**, *105*, 4702−4707.

(65) Hall, L. E.; Reimers, J. R.; Hush, N. S.; Silverbrook, K. *J. Chem. Phys.* **2000**, *112*, 1510−1521.

(66) Vuillaume, D.; Chen, B.; Metzger, R. M. *Langmuir* **1999**, *15*, 4011−4017.

(67) Budavari, S., Ed. *The Merck Index*; 12th ed.; Merck & Co., Inc.: Whitehouse Station, PA, 1996.

(68) Campbell, I. H.; Rubin, S.; Zawodzinski, T. A.; Kress, J. D.; Martin, R. L.; Smith, D. L.; Barashkov, N. N.; Ferraris, J. P. *Phys. Rev. B* **1996**, *54*, 14321−14324.

(69) Gershewitz, O.; Grinstein, M.; Sukenik, C. N.; Regev, K.; Ghabboun, J.; Cahen, D. *J. Phys. Chem. B* **2004**, *108*, 664−672.

(70) Delerue, C.; Cleri, F. Institut d'Electronique, Micro-électronique et Nanotechnologie, CNRS "Theoretical Physics Group", Villeneuve d'Ascq, France. Private communication.

(71) Schottky, W. *Naturwissenschaften* **1938**, *26*, 843.

(72) Mott, N. F. *Proc. Cambr. Philos. Soc.* **1938**, *34*, 568.

(73) Bardeen, J. *Phys. Rev.* **1947**, *71*, 717.

(74) Cowley, A. M.; Sze, S. M. *J. Appl. Phys.* **1965**, *36*, 3212−3220.

(75) UPS experiments are in progress.

(76) Vazquez, H.; Oszwaldowski, R.; Pou, P.; Ortega, J.; Perez, R.; Flores, F.; Kahn, A. *Europhys. Lett.* **2004**, *65*, 802−808.

(77) Shen, C.; Hill, I.; Kahn, A. *J. Am. Chem. Soc.* **2000**, *122*, 5391.

(78) Shen, C.; Kahn, A.; Schwartz, J. *J. Appl. Phys.* **2001**, *89*, 449.

(79) Fisher, G. L.; Walker, A. V.; Hooper, A. E.; Tighe, T. B.; Bahnck, K. B.; Skriba, H. T.; Reinard, M. D.; Haynie, B. C.; Opila, R. L.; Winograd, N.; Allara, D. L. *J. Am. Chem. Soc.* **2002**, *124*, 5528−5541.

(80) Walker, A. V.; Tighe, T. B.; Cabarcos, O. M.; Reinard, M. D.; Haynie, B. C.; Uppili, S.; Winograd, N.; Allara, D. L. *J. Am. Chem. Soc.* **2004**, *126*, 3954−3963.

(81) Walker, A. V.; Tighe, T. B.; Reinard, M. D.; Haynie, B. C.; Allara, D. L.; Winograd, N. *Chem. Phys. Lett.* **2003**, *369*, 615−620.

(82) Fisher, G. L.; Hooper, A. E.; Opila, R. L.; Allara, D. L.; Winograd, N. *J. Phys. Chem. B* **2000**, *104*, 3267−3273.

(83) Jung, D. R.; Czanderna, A. W. *Crit. Rev. Solid State Mater. Sci.* **1994**, *191*, 1−54.

(84) Ahn, H.; Whitten, J. E. *J. Phys. Chem. B* **2003**, *107*, 6565−6572.

(85) Crispin, X.; Geskin, V.; Crispin, A.; Cornil, J.; Lazzaroni, R.; Salaneck, W. R.; Brédas, J. L. *J. Am. Chem. Soc.* **2002**, *124*, 8131−8141.

(86) Kornilovitch, P. E.; Bratkovsky, A. M.; Williams, R. S. *Phys. Rev. B* **2002**, *66*, 165436.

(87) *NIST Chemistry WebBook*; National Institute of Standards and Technology (NIST): Gaithersburg, MD, 2005; available at http://webbook.nist.gov/chemistry/ (accessed Nov 2005).

(88) Tran Van, F. Laboratoire de Physicochimie des Polymères et des Interfaces, Université de Cergy-Pontoise, Cergy-Pontoise, France. Unpublished data, 2004.

(89) Skotheim, T. A., Ed. *Handbook of Conducting Polymers*; Marcel Dekker: New York, 1986; Vol. 2.